Soft Matter

PAPER

View Article Online
View Journal

Cite this: DOI: 10.1039/d4sm00516c

Elucidating the role of physicochemical interactions on gel rheology

Elnaz Nikoumanesh, Charles Joseph M. Jouaneh and Ryan Poling-Skutvik *

Received 30th April 2024,
Accepted 24th June 2024

DOI: 10.1039/d4sm00516c

rsc.li/soft-matter-journal

Soft materials are characterized by their intricate interplay of structure, dynamics, and rheological properties. This complexity makes it challenging to accurately predict their response to shear stress. Here, we investigate how the nature of bonds – electrostatic attractions, physical entanglements, physical repulsion, and covalent bonds – affects the linear and nonlinear rheology of gels. Specifically, we determine the critical roles these bonds play in the yield transition and thixotropic recovery of gel properties through a combination of linear oscillatory deformations, serial creep divergence measurements, and time-resolved flow sweeps. Different classes of gels are prepared with nearly identical linear rheology but significantly different yield transitions and nonlinear properties post-yielding. These differences are directly related to the kinetics by which the underlying elastic networks rebuild after flow. Gels which exhibit thixotropic hysteresis are able to fully recover their yield stress over time while non-thixotropic gels possess time-independent yielding metrics. This direct comparison between thixotropy and yielding reveals the intimate relationship between these phenomena and their controlling physical mechanisms within soft, amorphous materials.

1 Introduction

Gels are a class of materials characterized by their mechanical properties between those of liquids and solids.[1] At rest, gels possess a percolating network that elastically deforms to support small applied stresses and that suppresses relaxations.[2] When subjected to a large stress, however, the gel network breaks down to facilitate flow and viscously dissipates energy.[3–5] This transition from elastic deformation to viscous flow is known as the yield transition and is most commonly associated with a finite strain or stress.[6–8] Even though the yield transition is ubiquitous and critically important for many industrial processes,[9,10] there remains significant ambiguity over how to define and quantify "the" yield stress σ_y or yield strain γ_y.[11]

Recent insights into this phenomenon reveal that some of the ambiguity arises from the fact that the yield transition is a continuous rather than instantaneous process.[12] In this continuous framework, materials accumulate finite plastic strain during deformation, eventually resulting in network failure. Furthermore, as flow develops, shear forces may result in the remodeling and breakdown of the fluid structure. If this structural change is reversible, the elastic network reforms over time once the flow is suppressed, and this reformation is referred to as thixotropy.[13,14] Although many yield-stress materials exhibit thixotropy, these phenomena are distinct in their origins with thixotropy being time-dependent while yielding is stress-dependent. Nevertheless, these observations indicate that both yielding and thixotropy are inherently dynamic processes facilitated by the rearrangement of gel constituents coupled with external stresses and deformations. Thus, it becomes essential to understand the nature of the physicochemical bonds connecting these particulates into a cohesive elastic network to predict their yielding and thixotropic properties.[15]

Broadly, thixotropic yield stress fluids can be prepared from a wide variety of constituent building blocks with varying interparticle potentials and geometries.[13] In the case of small aspect ratio particles such as spheres or rods, elastic networks are formed through repulsive or attractive potentials. In a repulsive paradigm, yield stress fluids develop through the jamming of hard or soft particles at high volume fractions so that the particle size and elasticity control elasticity.[16–18] This elastic transition can occur at low volume fractions for highly charged species in which long-range electrostatic repulsion facilitates the formation of a Wigner glass.[19] By contrast, in an attractive paradigm, an elastic network results from the growth and percolation of fractal clusters either through diffusion-limited or reaction-limited aggregation.[20–23] In gels with either attractive or repulsive interactions, the gel strength and elasticity depend strongly on the concentration and strength of the resulting bonds. Particles with specific interactions or patches tend to form more complex structures due to their ability to explore a wider range of energy landscapes during assembly.[24,25] Additionally, fibers or polymer chains possess elongated, high aspect ratio conformations that

Department of Chemical Engineering, University of Rhode Island, Kingston, RI 02881, USA. E-mail: ryanps@uri.edu

allow the particulates to interpenetrate and develop elasticity through physical entanglements.[26,27] Finally, covalent networks can be formed through multifunctional crosslinkers.[28] In contrast to other interaction profiles, covalent crosslinking results in an irreversible bond that once broken under flow is not able to reform without additional reactants. Although theories postulate how these different interaction profiles and structural moieties build elasticity, their impact on nonlinear rheology through yield transition and thixotropic recovery remains poorly understood.

Here, we prepare gels possessing different physicochemical interactions – electrostatic attraction, physical entanglement, physical repulsion, and covalent crosslinking – but quantitatively similar linear rheological moduli. Despite their similar linear responses, these gels exhibit vastly different nonlinear properties which we quantify through serial creep divergence (SCD) rheology[29] and hysteresis loops in steady shear flow sweeps.[30,31] For attractive gels or gels possessing physical entanglements, we observe significant thixotropy and a time-dependent yield stress. For gels possessing physical repulsions and covalent crosslinks, we observe yield transitions characterized by a time-independent yield stress. We attribute the distinct nonlinear rheology of these gels to the different dynamics of constituent building blocks. For thixotropic gels, the time-dependent yield stress arises from the finite time scales associated with the coupled diffusion–aggregation of colloidal clusters or reptative re-entanglement of fibrillar networks. By contrast, time-independent yield stresses emerge for samples exhibiting minimal thixotropy due to either infinitely fast or infinitely slow recoveries for repulsive gels and covalent networks, respectively. These observations demonstrate that yielding and thixotropy are highly related phenomena that emerge from dynamic rearrangements of constitutive building blocks. Additionally, our findings demonstrate that SCD is a sensitive probe of dynamics in thixotropic yield stress fluids but that accurate interpretation of the recovery kinetics requires prior knowledge of dynamic modes.

2 Materials and methods

2.1 Materials

Cellulose nanocrystals (CNCs) were purchased from CelluForce (Montreal, Canada) as a dry powder, potassium chloride (KCl) was purchased from Fisher Scientific, Carbopol 940 was purchased from Lubrizol as a dry white powder, 4-(4,6-dimethoxy-1,3,5-triazin-2-yl)-4-methyl-morpholinium chloride (DMTMM) and hexamethylenediamine (HMDA) were purchased from Sigma-Aldrich, and TEMPO-oxidized cellulose nanofibers (CNFs) were purchased from the University of Maine. All materials were used as received.

2.2 Gel preparation

To test the effect of different physicochemical interactions on gel rheology, we prepared four different classes of samples (Fig. 1). First, we prepared electrostatically attractive CNC gels by adding KCl to destabilize the colloidal suspension. Second, we prepared physically entangled CNF gels by evaporating solvent to increase the fibril concentration. Third, we prepared gels with physically repulsive gels by dissolving Carbopol at sufficiently high concentrations. Finally, we crosslinked the carboxylic acid groups on the surface of CNFs with diamines to form a covalently linked gel. Additional details on each sample are provided below.

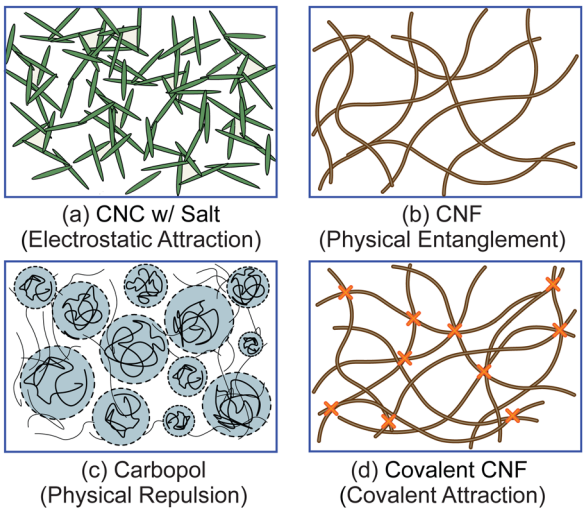

Fig. 1 Schematic illustrating the structures of the four classes of gels: (a) a CNC gel experiencing electrostatic attractions, (b) a CNF gel with physical entanglements, (c) a Carbopol gel with physical repulsion, and (d) a CNF gel with covalent crosslinks.

2.2.1 Electrostatically attractive CNC gels. To prepare the CNC sample, we followed our earlier procedure[29] in which CNCs are dispersed in deionized water and stirred on a stir plate until clear, indicating a uniform and homogeneous suspension. Then, a solution of KCl was added to form a sample with a final concentration of 30 mM KCl and 3 wt% CNC. The gels were then allowed to homogenize overnight on a tube roller.

2.2.2 Physically entangled CNF gels. CNFs were received as an approximately 1 wt% suspension in water. A rotary evaporator was used to remove excess water and obtain an approximately 3 wt% gel. The sample remained optically transparent and visually homogeneous throughout the evaporation protocol.

2.2.3 Physically repulsive Carbopol gels. Carbopol was dispersed in deionized water at a concentration of 1 wt% and stirred for an hour using a magnetic stirrer. The result was a hazy and viscous liquid with an initial pH of about 4. To adjust the pH, sodium hydroxide (NaOH) solution was added and the mixture was stirred manually until the pH stabilized at approximately 7.[32] The neutralized gel was visually uniform and optically transparent.

2.2.4 Covalently crosslinked CNF gels. To crosslink the CNF fibers, we developed a procedure that reacts the carboxylic acids present on the CNF surface to primary amines.[33] Briefly, the CNF suspension, with a charge density of 1.48 mmol g^{-1} of dry CNF, was concentrated using a rotary evaporator to a concentration of 2 wt%. Then, a stock solution of DMTMM coupling reagent was added to the concentrated CNF suspension at a stoichiometric ratio to carboxylic acid groups.[33] Lastly, HMDA was added at a 0.4 : 1 molar ratio to carboxylic acid groups on the CNF, resulting in a 0.8 : 1 molar ratio of $COOH : NH_2$ along with sufficient water to prepare a final gel at 1 wt%. All hydrogels were initially prepared by mixing the

aforementioned components in a 50 mL beaker and then casting the gel immediately into a 26 mm circular silicone mold.

2.3 Rheology

The rheological properties of these gels were assessed through a variety of rheological procedures. Rheological measurements were conducted using a TA Instruments HR20 rheometer. A solvent trap was employed to reduce evaporation during the experiments. To further mitigate evaporation, the edges of the samples were coated with mineral oil. All measurements were conducted at a constant temperature of $T = 25\ ^{\circ}C$.

2.3.1 Oscillatory measurements. Oscillatory measurements were conducted using a 40 mm diameter cross-hatched parallel plate geometry. We applied a series of amplitude sweeps to the sample, starting from a low to high strain γ followed by a reverse sweep at $\omega = 10$ rad s^{-1}. For the frequency sweeps, we selected a strain within the linear viscoelastic (LVE) region and measured the moduli as a function of frequency $10^{-1} \leq \omega \leq 10^{2}$ rad s^{-1} in both increasing and decreasing directions.

2.3.2 Serial creep divergence. The serial creep divergence (SCD) protocol followed our earlier work.[29,34] Briefly, we loaded samples onto a rheometer equipped with a 40 mm diameter cross-hatched parallel plate geometry and applied a constant shear rate of $\dot{\gamma} = 100$ rad s^{-1} for 1 minute. This pre-shear disrupted the underlying structural network in the material and erased previous mechanical history. After, we allowed the sample to rest under quiescent conditions for a waiting time t_w before imposing a stress σ and measuring the sample compliance. We repeated this procedure for increasing t_w and σ.

2.3.3 Time-resolved flow sweeps. For this experiment, we used a 60 mm parallel plate geometry to improve the signal at low shear rates and small averaging times. We followed existing procedures[30,31] to generate two flow curves. The first flow curve was collected by decreasing the shear rate from high shear $\dot{\gamma}_{max} = 10^{3}$ s^{-1} to low $\dot{\gamma}_{min} = 10^{-2}$ s^{-1} through $N = 8$ steps per decade with each step lasting for a duration of $3 \leq \delta t \leq 100$ s. We then immediately increased the shear rate back from $\dot{\gamma}_{min}$ to the initial value of $\dot{\gamma}_{max}$. By controlling the time at each shear rate, the average shear stress reflected changes in the sample structure.

3 Results and discussion

Because of the variety of rheological protocols used in this work, we provide a quick overview of our results before discussing each finding in detail below. First, using linear frequency sweeps, we verify that the four classes of gels investigated here – electrostatically attractive CNC, physically entangled CNF, physically repulsive Carbopol, and covalently crosslinked CNF – exhibit quantitatively similar viscoelastic relaxations. Second, we identify that each of these gels exhibits the expected yield transition with increasing stress under oscillatory and steady shear deformations. Third, by conducting SCD protocols, we identify that this yield transition depends strongly on shear history for electrostatically attractive CNC and physically entangled CNF gels but is independent of shear history for physically repulsive Carbopol gels. For covalently bonded CNF gels, the yield transition is unique for the first yielding event and then becomes independent of shear history for subsequent yielding. Lastly, we reconcile these different yielding kinetics by quantifying the magnitude of thixotropic hysteresis in time-resolved flow sweeps.

3.1 Linear frequency sweeps

We conduct oscillatory rheology to quantify the linear viscoelastic properties of gels as a function of frequency ω. The linear moduli of gels depend strongly on the concentration of constituent species and effective bond density.[35] By varying the concentrations of salt, constituent species, and crosslinker, we prepare gels that exhibit quantitatively similar relaxation spectra despite their different physicochemical compositions, as shown in Fig. 2. For each gel, the storage modulus G' is nearly independent of frequency, varying by less than an order of magnitude over four decades in frequency, with a value of $G' \approx 300$ Pa. Additionally, the loss modulus G'' is significantly lower than G', resulting in $\tan(\delta) = G''/G' \approx 0.1$ for all samples without a strong dependence on ω. These results confirm that the various classes of gels are viscoelastic solids with suppressed relaxations. Furthermore, the linear rheology of these gels is nearly indistinguishable across the gel classes, providing us with an ideal comparison to evaluate the role of physicochemical interactions in their nonlinear response.

3.2 Yielding response

After confirming that these gels exhibit similar linear relaxation spectra, we now assess how different interactions modify their nonlinear response. As an initial test, we apply oscillatory deformations at a fixed frequency ($\omega = 10$ rad s^{-1}) and varying strain γ (Fig. 3). With increasing γ (*i.e.*, an up-sweep), each gel

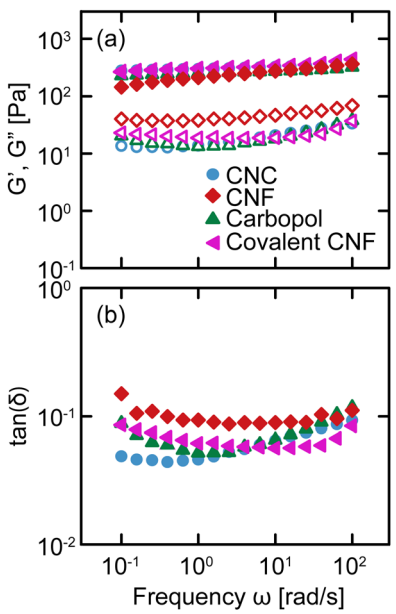

Fig. 2 (a) Storage (closed symbols) G' and loss (open symbols) G'' moduli and (b) $\tan(\delta) = G''/G'$ as a function of frequency ω for the four classes of gels: CNC, entangled CNF, Carbopol, and covalent CNF.

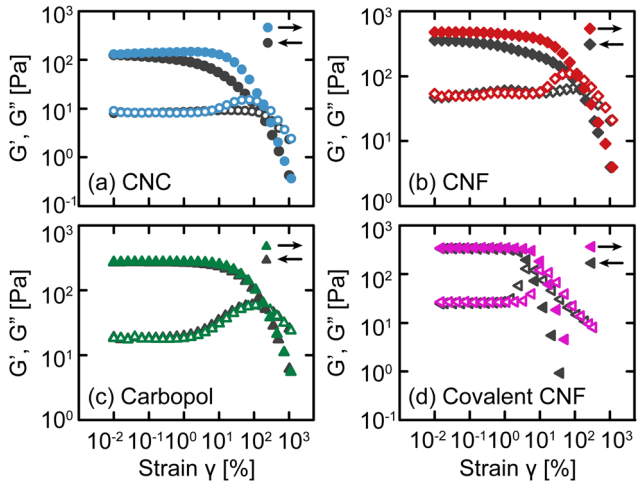

Fig. 3 Storage (closed symbols) G' and loss (open symbols) G'' moduli as a function of oscillatory strain γ for the four classes of gels: (a) CNC, (b) entangled CNF, (c) Carbopol, and (d) covalent CNF. Data collected with increasing and decreasing γ are shown in color and gray, respectively.

undergoes a yield transition. At small γ, the materials deform linearly with G' and G'' that are independent of γ, but at larger γ, G' decreases rapidly and G'' experiences an overshoot associated with the accumulation of unrecoverable strain.[12,36] These responses confirm that the gels yield under sufficiently high stress to transition from solid-like to liquid-like behavior.

After the samples have fully yielded so that $G'' > G'$, we continue to apply oscillatory deformations but with decreasing γ (*i.e.*, a down-sweep). For simple viscoelastic materials, the down-sweep and up-sweep measurements should agree because the moduli act as state variables dictated by ω and γ. While this is true for Carbopol gels, confirming that they form simple yield stress fluids,[37,38] the amplitude sweeps disagree for the electrostatically attractive CNC, physically entangled CNF, and covalent CNF gels, especially around the G'' overshoot. For the CNC and entangled CNF gels, the G'' overshoot is almost completely missing from the down-sweep and G' is only fully recovered at very small strains. We attribute these differences to the kinetics of colloidal and fibrillar rearrangements from the fluidized state at a high γ to the gel state at a low γ. Once the network fluidizes,[39] there is a finite time scale associated with network reformation as CNCs or CNFs diffuse and re-aggregate or re-entangle, respectively. Thus, the difference between up- and down-sweeps reflects the evolving structure of the sample post-yielding.

The covalent CNF gel has similar but qualitatively distinct differences between the up- and down-sweeps; the G'' overshoot is preserved, and G' recovers entirely at a relatively high γ. Whereas the CNC and entangled CNF gels possess recoverable bonds, the covalent CNF network can only yield by breaking chemical bonds either along the cellulose backbone or the amide bond formed between the diamine crosslinker and carboxylic acid groups on the CNF surface. Once broken, these bonds cannot reform and therefore the network cannot recover. Surprisingly though, the linear elastic modulus of this covalent network fully recovers after yielding despite the network losing some fraction of bonds during flow. Instead, the weaker network manifests through a decrease in the yield strain γ_y (and therefore in the the yield stress σ_y), quantified by the crossover between G' and G''. This initial finding suggests that nonlinear properties may be a more sensitive metric to assess gel strength and shear history dependence than the standard linear recovery measurements after step changes in shear strain or rate.[40,41]

The sensitivity of yielding to shear history is further investigated through creep measurements in which samples are subjected to a constant stress rather than a sinusoidal strain. Whereas strain-controlled oscillatory measurements require the sample to deform a specified magnitude, deformation in creep is accumulated over time as the material responds to the applied stress. Here, we measure the compliance $J = \gamma/\sigma$ of freshly prepared gels as a function of time under different values of stress σ spanning the yield stress σ_y (Fig. 4). Across different gel classes, we observe qualitatively similar behavior. At low σ, gels deform elastically with very weak time dependence consistent with previous measurements on colloidal gels.[42] As σ increases, the gel compliance increases more rapidly with time as unrecoverable strain accumulates.[12] At a sufficiently high σ, the samples yield under stress with a dramatic increase in their compliance as their elastic structure fluidizes. After the samples have yielded, subsequent creep measurements result in viscous flow in which the compliance scales with time as $J = t/\eta$ in which η is the effective viscosity of the fluidized gel.[43] This viscous flow indicates that the structural network of the gel breaks down during the yield transition.

In addition, this structural change is inferred from the difference in the creep ringing response of gels pre- and post-yielding. Creep ringing refers to the underdamped oscillations observed at small times as a result of the coupling of instrument inertia to material elasticity.[44] Oscillations only appear when the material elasticity is sufficiently high relative to the sum of viscous and applied stresses.[45,46] For all gels, the oscillations disappear when $\sigma > \sigma_y$, indicating an overdamped response. For the CNC, entangled CNF, and covalent CNF gels, we attribute this overdamped response to lower gel elasticities resulting from structural breakdown, supported by the significantly higher compliance values measured for post-yielded samples. By contrast, the compliance of Carbopol gels agrees at short times with the pre-yielded samples, indicating that the network elasticity is maintained across the yield transition. The overdamped response thus emerges because the applied stress dominates the material elasticity. These creep measurements thus further suggest that the yield transition is highly sensitive to the structural breakdown and recovery facilitated by physicochemical interactions between constituents and their resulting rearrangements.

3.3 Serial creep divergence (SCD)

To probe the kinetics of structural breakdown and recovery, we conduct SCD measurements.[29,34] SCD is a rheological protocol designed to quantify the yield transition in the presence of thixotropy by applying creep deformations as a function of

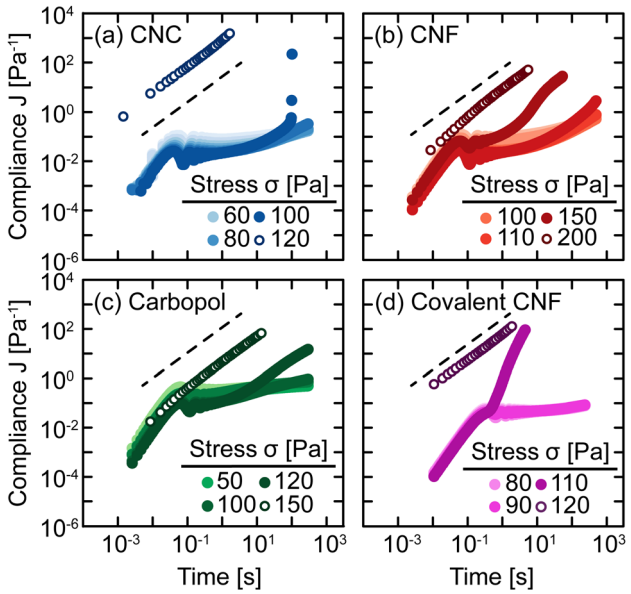

Fig. 4 Compliance $J = \gamma/\sigma$ as a function of time for (a) CNC, (b) entangled CNF, (c) Carbopol, and (d) covalent CNF gels at different stresses. Open symbols indicate experiments conducted after the first yielding event. Dashed lines indicate linear scaling $J \sim t$.

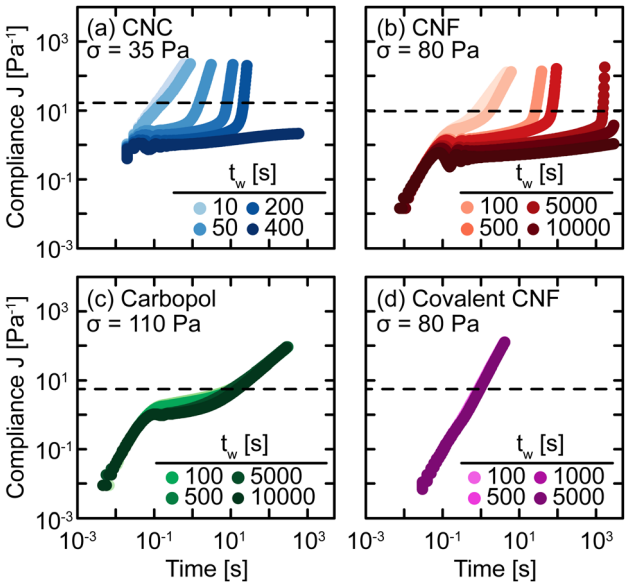

Fig. 5 Compliance $J = \gamma/\sigma$ as a function of time at constant stress σ for various waiting times t_w after yielding for (a) CNC, (b) entangled CNF, (c) Carbopol, and (d) covalent CNF gels. Dashed lines indicate the creep threshold J^* used to identify the yield time Δt_y.

waiting time t_w after yielding. Briefly, this procedure consists of pre-shearing the samples to remove shear history effects and to initialize the gel structure. After this pre-shear, the sample is allowed to rest quiescently for a set time period t_w. Then, the sample is subjected to a constant stress σ to measure the compliance as a function of time. The yield time Δt_y is determined as the time at which the compliance J crosses an arbitrary threshold J^* that distinguishes between primary creep and viscous flow behaviors. If $\Delta t_y \ll t_w$, the SCD measurement provides quasi-instantaneous characterization of the gel strength. By tracking the evolution of Δt_y with t_w and σ, we build a comprehensive understanding of yielding and structural recovery.

SCD measurements are performed on all gel classes, as shown in Fig. 5. At short t_w, the gels exhibit a nearly constant power law increase in compliance, indicating that the samples immediately flow through a combination of viscous dissipation, characterized by the scaling $J \sim t$, and instrument inertia, characterized by the scaling $J \sim t^2$. This rapid increase in compliance indicates that while these materials are elastic at rest (Fig. 2), the pre-shear protocol and forced yielding destroy the underlying elastic network with insufficient time for the network to recover. For the Carbopol gel, however, there is an intermediate plateau present even for the shortest t_w measured. This difference in short time behavior indicates that the elastic network in Carbopol gels is restored nearly instantaneously after yielding, consistent with the lack of hysteresis in oscillatory amplitude sweeps (Fig. 3) and the agreement observed in the creep ringing regime (Fig. 4).

As t_w increases, the CNC and entangled CNF gels begin to exhibit intermediate plateaus in their creep response. These plateaus indicate that the gels temporarily support the applied stress through a partial recovery of their underlying elastic network, consistent with the substantial hysteresis observed for these materials in oscillatory amplitude sweeps (Fig. 4(a and b)). After a long t_w, the network sufficiently restructures to fully support σ, resulting in persistent long-time plateaus. For example, the compliances of CNC and entangled CNF gels after t_w = 400 s or 10 000 s, respectively, no longer exhibit upturns to cross J^*. We observe qualitatively different behavior for Carbopol and covalently cross-linked CNF gels in which there is no significant change in J as a function of t_w. For Carbopol, we associate this temporal independence to a nearly instantaneous recovery of elasticity after yielding; because the network is formed by physical repulsion, once the polymeric microgels viscously rearrange during flow, they immediately re-enter a free energy minimum formed by a cage of nearest neighbors.[47,48] For covalent CNF networks, we attribute this behavior to the opposite effect in which the structure is permanently destroyed under flow. In contrast to the instantaneous recovery in Carbopol, the breaking of covalent bonds results in effectively infinitely long recovery times unless more reactants and catalysts are present to restore the broken covalent bonds. This picture is supported by the fact that after preshearing, the covalent CNF gels yield and flow at much lower stresses than the neat gel *i.e.*, σ = 80 Pa in SCD but $\sigma \approx$ 110 Pa in creep (Fig. 4). Surprisingly, this decrease in the apparent yield stress of the covalent CNF contrasts with the recovery in linear elasticity observed in Fig. 3, suggesting that non-linear rheological metrics are more sensitive to structural changes in the material than linear properties.

The qualitative changes observed in SCD can be quantified by defining the yield time Δt_y as the difference between the time at which $J(t) = J^*$ and the inertial response of the instrument (see ref. 29 for specifics), which we plot as a function of t_w and applied stress σ in Fig. 6. For all samples, we observe a

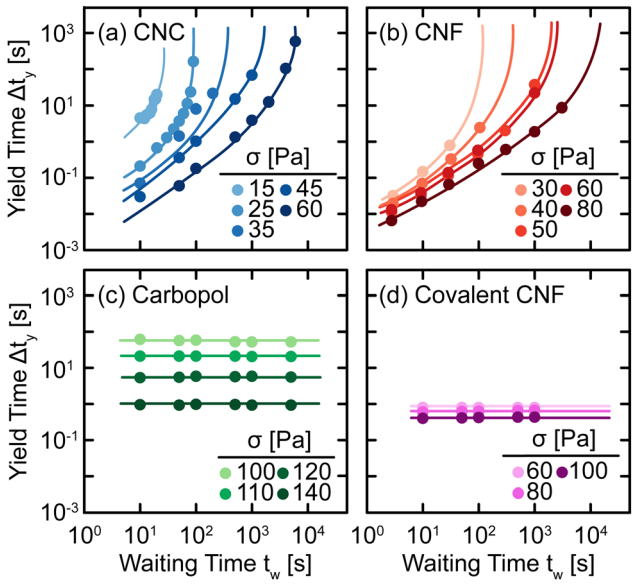

Fig. 6 Yield time Δt_y as a function of waiting time t_w under different applied stresses σ for (a) CNC, (b) entangled CNF, (c) Carbopol, and (d) covalent CNF gels. Curves are guides to the eye.

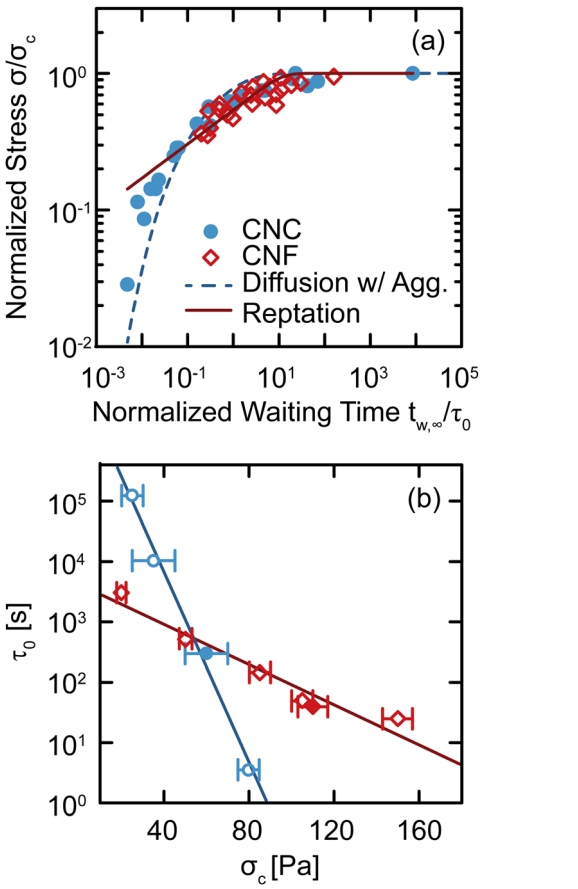

Fig. 7 (a) Normalized stress σ/σ_c as a function of the normalized divergent waiting time $t_{w,\infty}/\tau_0$ for CNC and entangled CNF gels. The dashed line shows the best fit to the diffusion–aggregation model (eqn (2)) and the solid line is the best fit to the reptation model (eqn (3)). (b) Normalization time scale τ_0 as a function of critical stress σ_c. Solid lines are exponential fits. Closed symbols are from this work and open symbols are from our earlier work on CNC gels[29] and entangled CNF gels.[34]

decrease in Δt_y with respect to σ as higher stress causes the elastic networks to fail more rapidly. This stress-activated failure is commonly observed in associating suspensions[49,50] and polymer networks.[51,52] Additionally, for CNC and entangled CNF gels, we observe an increase in Δt_y with t_w as the elastic network rebuilds during quiescent rest. Once the elastic networks sufficiently recover, the samples no longer yield on experimental time scales and thus, Δt_y diverges at a finite t_w. By contrast, there is no significant change in Δt_y for Carbopol and covalent CNF gels, confirming that there is no structural recovery in these systems.

3.4 Restructuring kinetics

The changes observed in SCD demonstrate that there are unique restructuring kinetics across different classes of gels. We gain insight into these kinetics by recognizing that the time $t_{w,\infty}$ at which Δt_y diverges physically represents the time necessary for the gel constituents to form a network with a yield stress equal to the applied stress σ. Thus, by inverting the relationship and tracking how σ depends on $t_{w,\infty}$, we explicitly quantify the kinetics by which the gel structure rebuilds after yielding (Fig. 7(a)). For both CNC and entangled CNF gels, the kinetics collapse onto separate master curves by normalizing the applied stress by a critical stress σ_c, which represents the limit of network yield stress,[29] and normalizing the divergent yield times by a kinetic timescale τ_0, which describes constituent rearrangements. With these normalized variables, we observe an increase in the stress that the CNC and entangled CNF gels can withstand as the waiting time increases. This increase in stress follows the restructuring kinetics of the elastic network after yielding. Furthermore, by combining the results of this study with SCD results from our earlier investigations,[29,34] in which we varied constituent concentrations to prepare gels with different critical stresses σ_c, we show that the normalization time scale τ_0 decreases exponentially σ_c according to $\tau_0 \sim \exp(-\sigma_c/\sigma_\tau)$, where $\sigma_\tau = 5.5 \pm 0.4$ Pa and 26 ± 3 Pa for CNC and CNF gels, respectively (Fig. 7(b)). This decrease in τ_0 with σ_c indicates that stiffer gels recover their yield stress more rapidly.

Further insight into the physics of this relationship can be gained by modeling the restructuring kinetics according to constituent dynamics. Our kinetic modeling assumes that these thixotropic gels yield by forming shear bands in which the shear stress is localized to a narrow interface between plug-like regions. Shear banding is commonly observed for thixotropic yield stress fluids[3,53–57] and is predicted theoretically.[58,59] With this assumption, the network should rebuild through the Brownian motion of constituents across this shear band interface and reintegration into the cohesive elastic network preserved within each shear band. Although these models were developed in earlier work, they demonstrate the specific physical mechanisms underlying thixotropy, allowing us to contrast thixotropic kinetics across different physicochemical interactions.

3.4.1 Attractive colloidal gels: diffusion–aggregation. For attractive colloidal systems (*i.e.*, CNC gels), we assume that

individual colloids undergoing Brownian motion move diffusively with diffusivity D_0. Thus, we describe the spatiotemporal evolution of particle concentration according to Fick's second law in one-dimension:

$$\frac{\partial c}{\partial t} = D_0 \frac{\partial^2 c}{\partial x^2}. \quad (1)$$

By assuming that these gels fail at a shear band interface and recover through the growth of fractal clusters, we solve this differential equation to get

$$\frac{\sigma_c - \sigma}{\sigma_c} = \frac{4}{\pi} \sum_{n=\text{odd}}^{\infty} \frac{1}{n} \sin\left(\frac{n\pi}{2}\right) \exp\left[-\frac{n^2\pi^2\zeta_0}{4(0.45)}\left(\frac{t}{\tau_0}\right)^{0.45}\right], \quad (2)$$

where ζ_0 is a fitting parameter related to the width of the shear band interface. We provide a complete derivation of this solution in our earlier work.[29] This diffusion–aggregation model excellently fits our experimental findings (Fig. 7(a)), confirming our hypothesis that these gels fail by yielding at a shear band interface. In this physical picture, the decrease in τ_0 with increasing σ_c indicates a decrease in the width of the shear band interface.

3.4.2 Entangled fibrillar gels: reptation. The entangled CNF gels exhibit similar restructuring kinetics to those of the CNC gels but with very different constituent structures – elongated fibers instead of anisotropic colloids. Therefore, we assume that the CNF gels yield through a similar shear banding mechanism but with different recovery kinetics. The extended conformation of CNF fibers resembles that of high molecular weight polymers and the recovery kinetics can therefore be modeled according to the existing reptation theories.[60,61] In these models, the planar chain density ρ across an interface follows

$$\frac{\rho(t)}{\rho_\infty} = \frac{2}{\sqrt{\pi}}\left(\sqrt{\tau} + 2\sum_{k=1}^{\infty}(-1)^k \times \left[\sqrt{\tau}\exp\left(\frac{-k^2}{\tau}\right) - \sqrt{\pi}k\,\text{erfc}\left(\frac{k}{\sqrt{\tau}}\right)\right]\right), \quad (3)$$

where $\tau = 2t/\tau_0 N^2$, N is the number of segments per chain, and ρ_∞ is the chain density at equilibrium. By accounting for the energy of chain pullout[62,63] and Griffith's fracture criterion,[64] the yield stress can be derived as $\sigma(t)/\sigma_c = (\rho(t)/\rho_\infty)^{1/2}$. Full details of this derivation can be found in our previous work.[34] This expression excellently fits the increase in gel strength for entangled CNFs (Fig. 7(a)), confirming that the entangled CNF gels recover their yield stress through re-entanglements across the shear band interface.

Although these models for the coupled diffusion–aggregation of attractive colloids and reptative re-entanglement of fibers across a shear band interface predict the measured increase in the yield stress of these gels, there are surprisingly small quantitative differences between the kinetics of these two gel classes. For example, for $t_{w,\infty}/\tau_0 > 10^{-1}$, the measured values and model predictions are nearly indistinguishable (Fig. 7(a)). Significant differences do appear, however, on shorter time scales where reptative re-entanglement predicts an order-of-magnitude larger yield stress than diffusion–aggregation. The similarity between these models demonstrates one limitation of the SCD procedure; it is challenging to isolate the specific restructuring mechanisms unless the constituent interactions and conformations are well understood. Nevertheless, SCD reveals that the attractive CNC and entangled CNF gels undergo nearly complete structural recovery after yielding if given sufficient time.

3.5 Thixotropic recovery

Up to this point, we have attributed changes in the response of gels post-yielding to structural recovery, *i.e.*, thixotropy. We now explicitly test this hypothesis using an established rheological protocol.[30,31] Briefly, this protocol consists of conducting flow sweeps from high shear rates $\dot{\gamma}$ to low and back using $N = 8$ steps per decade and averaging over a time interval δt ranging from 3 s to 100 s per step. This protocol results in flow sweeps with different magnitudes of hysteresis depending on the gel class, as shown in Fig. 8. For the CNC and entangled CNF gels, which show an increase in yield stress with waiting time, we observe significant differences between the flow sweeps in the up and down directions. By contrast, there is no significant difference between the Carbopol and covalent CNF gels, consistent with the time-independent yield stress measured in SCD. Furthermore, the intercepts of these flow curves should correspond to the dynamic yield stress of the gels. This intercept is comparable to σ_c for Carbopol, consistent with a lack of structural change during flow, but significantly lower than σ_c for the other gel classes. This suppressed yield stress is consistent with the expected structural breakdown during flow, which is recoverable for CNC and entangled CNF gels but irrecoverable for the covalent CNF gels.

The magnitude of rheological hysteresis is quantified through the logarithmic area A_σ between the down and up sweeps according to

$$A_\sigma = \int_{\dot{\gamma}_{min}}^{\dot{\gamma}_{max}} |\Delta\sigma(\dot{\gamma})| \mathrm{d}(\log(\dot{\gamma})) \quad (4)$$

where $\Delta\sigma(\dot{\gamma}) = \sigma_{up}(\dot{\gamma}) - \sigma_{down}(\dot{\gamma})$ and larger values of A_σ correspond to higher degrees of thixotropy. This logarithmic integration appropriately weighs contributions from a low and a high $\dot{\gamma}$. Consistent with the existing literature,[30,31,65] taking the absolute value of $\Delta\sigma$ guarantees that any difference in stress contributes to A_σ rather than canceling out, but it does obscure directional dependence. Typically, thixotropic fluids are more structured at a low $\dot{\gamma}$,[66,67] so stepping up from a low $\dot{\gamma}$ to a high $\dot{\gamma}$ should result in a higher σ than stepping down from high to low. Nevertheless, we calculate A_σ using trapezoidal numerical integration as a function of δt (Fig. 9). To compare the magnitude of hysteresis across gel classes, we normalize A_σ by σ_c. For the Carbopol and covalent CNF gels, we observe minimal hysteresis across all δt and attribute the small values of A_σ/σ_c to experimental errors. For the CNC and entangled CNF gels, however, we observe significantly larger values of A_σ/σ_c. Although we do not observe the non-monotonic peaks in A_σ that were identified in earlier investigations of thixotropic yield stress fluids,[30,31,65] the high magnitude of hysteresis observed

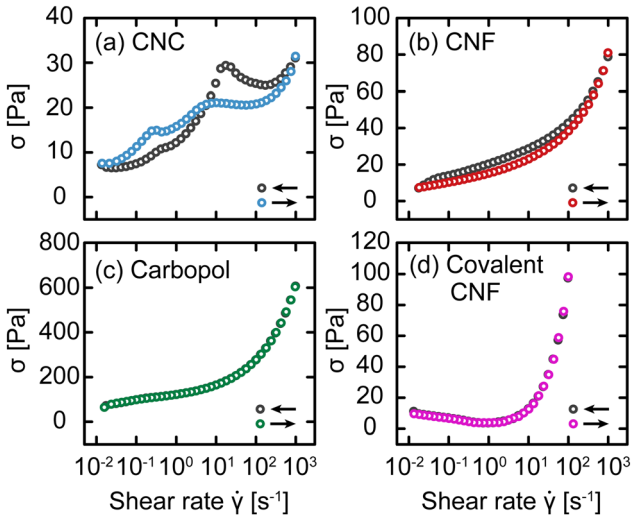

Fig. 8 Stress σ as a function of shear rate $\dot{\gamma}$ for (a) CNC, (b) entangled CNF, (c) Carbopol, and (d) covalent CNF gels with decreasing $\dot{\gamma}$ (gray) and increasing $\dot{\gamma}$ (color) with δt = 10 s.

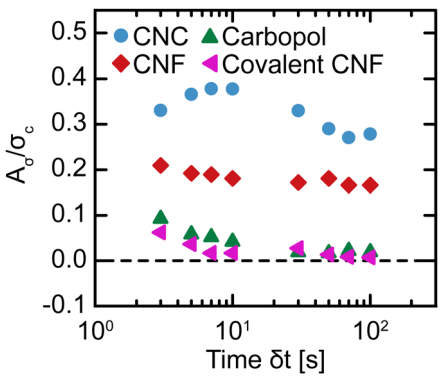

Fig. 9 Normalized hysteric area A_σ/σ_c as a function of the time interval per step δt in flow sweeps for different gel classes.

for these samples demonstrates that these gels are indeed thixotropic. Thus, only thixotropic gels possess time-dependent yield stresses while non-thixotropic gels exhibit constant yield stresses.

4 Conclusions

From our nonlinear rheological protocols, we observe various behaviors of gels post-yielding depending on their physicochemical interactions. For physically repulsive Carbopol gels, the elastic network recovers nearly instantaneously after yielding, resulting in negligible hysteresis between up and down sweeps and a time-independent yield stress. For covalent CNF gels, the elastic network is permanently destroyed locally upon yielding, also resulting in negligible hysteresis and a time-independent yield stress but with a significantly weaker yield stress after the first yielding event. For electrostatically attractive CNC and physically entangled CNF gels, we observe significant hysteresis and time-dependent yield stresses. After yielding, these gels dynamically rebuild their elastic structure and recover their yield stress through coupled diffusion–aggregation or reptative re-entanglement, respectively.

Through independent measurements of thixotropy and yielding, we demonstrate the intimate relationship between these two phenomena across different classes of gels. The effect of yielding on the linear and nonlinear properties of gels can vary drastically depending on the mechanisms by which the gels form a percolating elastic network. These effects can be best understood by considering the *dynamics* of the underlying constituents and the kinetics of bond reformation. Furthermore, we demonstrate that the yield stress is a more sensitive metric of network strength than linear properties. Whereas linear viscoelasticity may fully recover after yielding, the stress at which the gel fails may be significantly altered.

Data availability

Raw data for this article, including linear frequency sweeps, oscillation amplitude sweeps, creep compliance measurements, serial creep divergence rheology, and flow sweeps are available at Open Science Foundation at **https://doi.org/10.17605/OSF.IO/SYEZK**.

Conflicts of interest

There are no conflicts to declare.

Acknowledgements

This research was supported by the ACS Petroleum Research Fund Doctoral New Investigator Grant No. 65826-DNI9.

References

1 W. Richtering and B. R. Saunders, *Soft Matter*, 2014, **10**, 3695–3702.
2 H. H. Winter and F. Chambon, *J. Rheol.*, 1986, **30**, 367–382.
3 J. Colombo and E. Del Gado, *J. Rheol.*, 2014, **58**, 1089–1116.
4 S. Jamali, G. H. McKinley and R. C. Armstrong, *Phys. Rev. Lett.*, 2017, **118**, 048003.
5 A. Kurokawa, V. Vidal, K. Kurita, T. Divoux and S. Manneville, *Soft Matter*, 2015, **11**, 9026–9037.
6 N. J. Balmforth, I. A. Frigaard and G. Ovarlez, *Annu. Rev. Fluid Mech.*, 2014, **46**, 121–146.
7 A. Malkin, V. Kulichikhin and S. Ilyin, *Rheol. Acta*, 2017, **56**, 177–188.
8 D. P. Keane, C. J. Constantine, M. D. Mellor and R. Poling-Skutvik, *Langmuir*, 2023, **39**, 7852–7862.
9 D. Miranda-Nieves and E. L. Chaikof, *ACS Biomater. Sci. Eng.*, 2017, **3**, 694–711.
10 R. J. Mondschein, A. Kanitkar, C. B. Williams, S. S. Verbridge and T. E. Long, *Biomaterials*, 2017, **140**, 170–188.
11 H. A. Barnes, *J. Non-Newtonian Fluid Mech.*, 1999, **81**, 133–178.

12 G. J. Donley, P. K. Singh, A. Shetty and S. A. Rogers, *Proc. Natl. Acad. Sci. U. S. A.*, 2020, **117**, 21945–21952.
13 H. A. Barnes, *J. Non-Newtonian Fluid Mech.*, 1997, **70**, 1–33.
14 J. Mewis and N. J. Wagner, *Adv. Colloid Interface Sci.*, 2009, **147–148**, 214–227.
15 Y. Wang and R. H. Ewoldt, *J. Rheol.*, 2023, **67**, 1199–1219.
16 A. J. Liu and S. R. Nagel, *Annu. Rev. Condens. Matter Phys.*, 2010, **1**, 347–369.
17 T. K. Haxton, M. Schmiedeberg and A. J. Liu, *Phys. Rev. E: Stat., Nonlinear, Soft Matter Phys.*, 2011, **83**, 031503.
18 F. Khabaz, M. Cloitre and R. T. Bonnecaze, *Phys. Rev. Fluids*, 2018, **3**, 033301.
19 D. Bonn, H. Tanaka, G. Wegdam, H. Kellay and J. Meunier, *EPL*, 1999, **45**, 52–57.
20 T. Witten and L. Sander, *Phys. Rev. B: Condens. Matter Mater. Phys.*, 1983, **27**, 5686–5697.
21 M. Y. Lin, H. M. Lindsay, D. A. Weitz, R. C. Ball, R. Klein and P. Meakin, *Phys. Rev. A: At., Mol., Opt. Phys.*, 1990, **41**, 2005–2020.
22 V. Trappe, V. Prasad, L. Cipelletti, P. N. Segre and D. A. Weitz, *Nature*, 2001, **411**, 772–775.
23 S. Babu, J. C. Gimel and T. Nicolai, *Eur. Phys. J. E*, 2008, **27**, 297–308.
24 Z. Gong, T. Hueckel, G.-R. Yi and S. Sacanna, *Nature*, 2017, **550**, 234–238.
25 T. Zhang, D. Lyu, W. Xu, X. Feng, R. Ni and Y. Wang, *Nat. Commun.*, 2023, **14**, 8494.
26 R. Everaers, S. K. Sukumaran, G. S. Grest, C. Svaneborg, A. Sivasubramanian and K. Kremer, *Science*, 2004, **303**, 823–826.
27 J. Qin and S. T. Milner, *Macromolecules*, 2014, **47**, 6077–6085.
28 F. Chambon and H. Winter, *Polym. Bull.*, 1985, **13**, 499–503.
29 E. Nikoumanesh and R. Poling-Skutvik, *J. Chem. Phys.*, 2023, **159**, 044905.
30 T. Divoux, V. Grenard and S. Manneville, *Phys. Rev. Lett.*, 2013, **110**, 018304.
31 R. Radhakrishnan, T. Divoux, S. Manneville and S. M. Fielding, *Soft Matter*, 2017, **13**, 1834–1852.
32 M. Agarwal and Y. M. Joshi, *Phys. Fluids*, 2019, **31**, 063107.
33 C. A. Montalbetti and V. Falque, *Tetrahedron*, 2005, **61**, 10827–10852.
34 R. Poling-Skutvik, E. McEvoy, V. Shenoy and C. O. Osuji, *Phys. Rev. Mater.*, 2020, **4**, 102601.
35 M. Rubinstein and R. H. Colby, *Polymer Physics*, Oxford University Press, 2003.
36 K. Kamani, G. J. Donley and S. A. Rogers, *Phys. Rev. Lett.*, 2021, **126**, 218002.
37 T. Divoux, C. Barentin and S. Manneville, *Soft Matter*, 2011, **7**, 9335–9349.
38 M. Dinkgreve, M. Fazilati, M. M. Denn and D. Bonn, *J. Rheol.*, 2018, **62**, 773–780.
39 V. V. Vasisht, G. Roberts and E. Del Gado, *Phys. Rev. E*, 2020, **102**, 010604.
40 M. Zhang, D. Xu, X. Yan, J. Chen, S. Dong, B. Zheng and F. Huang, *Angew. Chem., Int. Ed.*, 2012, **51**, 7011–7015.
41 Z. Wei, J. H. Yang, J. Zhou, F. Xu, M. Zrínyi, P. H. Dussault, Y. Osada and Y. M. Chen, *Chem. Soc. Rev.*, 2014, **43**, 8114–8131.
42 J. H. Cho and I. Bischofberger, *Soft Matter*, 2022, **18**, 7612–7620.
43 R. G. Larson, *The Structure and Rheology of Complex Fluids*, Oxford University Press, 1999.
44 R. H. Ewoldt and G. H. McKinley, *Rheol. Bull.*, 2007, **76**, 4–6.
45 C. Baravian and D. Quemada, *Rheol. Acta*, 1998, **37**, 223–233.
46 C. Baravian, G. Benbelkacem and F. Caton, *Rheol. Acta*, 2007, **46**, 577–581.
47 Z. Zhou, J. V. Hollingsworth, S. Hong, H. Cheng and C. C. Han, *Langmuir*, 2014, **30**, 5739–5746.
48 N. Koumakis, M. Laurati, A. R. Jacob, K. J. Mutch, A. Abdellali, A. B. Schofield, S. U. Egelhaaf, J. F. Brady and G. Petekidis, *J. Rheol.*, 2016, **60**, 603–623.
49 C. Ligoure and S. Mora, *Rheol. Acta*, 2013, **52**, 91–114.
50 L. C. Johnson, B. J. Landrum and R. N. Zia, *Soft Matter*, 2018, **14**, 5048–5068.
51 L. Vanel, S. Ciliberto, P.-P. Cortet and S. Santucci, *J. Phys. Appl. Phys.*, 2009, **42**, 214007.
52 P. J. Skrzeszewska, J. Sprakel, F. A. de Wolf, R. Fokkink, M. A. Cohen Stuart and J. van der Gucht, *Macromolecules*, 2010, **43**, 3542–3548.
53 T. Divoux, D. Tamarii, C. Barentin and S. Manneville, *Phys. Rev. Lett.*, 2010, **104**, 208301.
54 O. Nechyporchuk, M. N. Belgacem and F. Pignon, *Carbohydr. Polym.*, 2014, **112**, 432–439.
55 T. Divoux, M. A. Fardin, S. Manneville and S. Lerouge, *Annu. Rev. Fluid Mech.*, 2016, **48**, 81–103.
56 D. Bonn, M. M. Denn, L. Berthier, T. Divoux and S. Manneville, *Rev. Mod. Phys.*, 2017, **89**, 035005.
57 R. Benzi, T. Divoux, C. Barentin, S. Manneville, M. Sbragaglia and F. Toschi, *Phys. Rev. Lett.*, 2019, **123**, 248001.
58 M. L. Manning, E. G. Daub, J. S. Langer and J. M. Carlson, *Phys. Rev. E: Stat., Nonlinear, Soft Matter Phys.*, 2009, **79**, 016110.
59 R. L. Moorcroft and S. M. Fielding, *Phys. Rev. Lett.*, 2013, **110**, 086001.
60 S. Prager and M. Tirrell, *J. Chem. Phys.*, 1981, **75**, 5194–5198.
61 R. P. Wool, B. L. Yuan and O. J. McGarel, *Polym. Eng. Sci.*, 1989, **29**, 1340–1367.
62 P. G. De Gennes, *Tribol. Ser.*, 1981, **7**, 355–367.
63 P. Prentice, *Polymer*, 1983, **24**, 344–350.
64 A. A. Griffith, *Philos. Trans. R. Soc. Math. Phys. Eng. Sci.*, 1921, **221**, 163–198.
65 S. Jamali, R. C. Armstrong and G. H. McKinley, *Phys. Rev. Lett.*, 2019, **123**, 248003.
66 Y. Wei, M. J. Solomon and R. G. Larson, *J. Rheol.*, 2019, **63**, 673–675.
67 R. G. Larson and Y. Wei, *J. Rheol.*, 2019, **63**, 477–501.